SPATIAL APPROACHES TO MOONS FROM RESONANCE RELATIVE TO INVARIANT MANIFOLDS

Rodney L. Anderson
Jet Propulsion Laboratory, California Institute of Technology, USA, rodney.l.anderson@jpl.nasa.gov

Martin W. Lo
Jet Propulsion Laboratory, California Institute of Technology, USA, martin.w.lo@jpl.nasa.gov

In this study, the final approach to a moon or other body from resonance is explored and compared to the invariant manifolds of unstable periodic orbits. It is shown that the stable manifolds of planar Lyapunov orbits can act as a guide for the periods or resonances that are required for the final approach in both the planar and spatial problems. Previously developed techniques for the planar problem are expanded for use with resonances and used for comparison with trajectories approaching a moon from these resonances. A similar technique is then used for exploring the relationship of invariant manifolds to approach trajectories in the spatial problem. It is shown that the invariant manifolds of unstable periodic orbits provide insight into the trajectory design, and they can be used as a guide to the more direct approach trajectories.

I. INTRODUCTION

Tying the last resonance in a tour to the final approach of a moon is currently one of the more challenging aspects of tour design. Often one of the chief characteristics of this final approach is that it is perturbed by multi-body effects in a highly nonlinear dynamic environment. The goal in the design of this final approach is not to simply overcome these effects, but to take advantage of them to reduce propellant requirements or to meet other mission constraints.

Various studies of the overall tour have been undertaken from a variety of different perspectives including those based on patched-conic methods,[1–3] optimization techniques,[4–7] and multi-body methods.[8–28] In each of these cases, the trajectories travel through multiple resonances, and it has been found that resonant orbits are important for ballistic, impulsive, and low-thrust trajectories.[25–27,29] See Anderson[30] for a more detailed discussion of the current status of resonance in tour design.

The final approach problem has often been solved separately from the rest of the tour, and it has typically required a separate set of tools. One of the earlier studies of the approach problem for mission design was done with Finlayson's PTool software.[31] It was used to design the final approach of the Europa Orbiter design developed by Sweetser et al.[32] and Johannesen and D'Amario[33] in 1999. Grebow, Petropoulos and Finlayson[34] further developed this technique to numerically search for trajectories approaching Europa. Lo[35] in 2001 and Grebow et al.[34] in 2011 noted that some desirable approach trajectories appear to heuristically follow invariant manifolds. Koon et al.[36] examined approaches to libration orbits via invariant manifolds near moons, and Topputo et al.[37] used invariant manifolds to search for transfers between planets. Lantoine also optimized trajectories that were traveling to halo orbits.[38] The general escape and capture problem has been examined by Villac and Scheeres,[39] Kirchbach et al.,[40] and Anderson and Lo.[41]

The results from these analyses have indicated that periodic orbits and their associated invariant manifolds may provide a platform from which to gain further understanding of the approach problem. Indeed, Poincaré indicated that periodic orbits are one of the keys to understanding the three-body problem,[42] and it is through this perspective that we intend to study the approach problem here. The planar approach problem was examined within the planar circular restricted three-body problem (CRTBP) in Anderson,[30] which provided a number of insights. It was shown that the invariant manifolds of planar Lyapunov orbits can be used to connect to different resonances as shown by the computation of multiple resonant orbits, and the connections to these resonances were explored for different systems. In Anderson and Parker[43] it was shown that the invariant manifolds of planar Lyapunov orbits act as general boundaries between trajectories approaching the Moon and originating at the Earth or Moon. In 2005, Anderson and Lo[41] examined the periods of collision orbit trajectories integrated backward in time from the secondary for short integration times, and distinct regions with different periods were observed.

The techniques used in these previous works for the planar problem are further developed here and applied to new cases in the planar problem. They are then expanded and used to analyze spatial approaches for trajectories starting from the apoapse opposite the secondary and including the very last portion of the approach. These spatial approaches are particularly challenging because the three-dimensional aspects of the problem present dif-

ficulties for the tools used to analyze the planar approach problem. Spatial approaches are also of particular importance since a number of trajectory designs that include science requirements use orbits with higher inclinations.[15] Only the final approach is considered here, and it is expected that it can be tied into the remainder of a tour design using other techniques. All of the methods used here are implemented in the three-body problem so that three-body effects may be included in the design from the initial portion of the design process. This method has the added benefit in that it provides additional insight into the dynamics and allows an analysis of the boundaries and parameters of the problem that will be useful for trajectory design.

II. MODELS

The two primary models used within this study are the CRTBP and the ephemeris model. The CRTBP has been shown to act as a good approximation for the ephemeris model in that trajectories computed in the CRTBP may typically be found in the ephemeris model. A number of useful tools and symmetries that facilitate the computations also exist in this problem. Additional trajectories may be found in the full ephemeris model, and this model is used for several specific analyses.

II.I. Circular Restricted Three-Body Problem

The majority of the periodic orbits and trajectories shown in this analysis are computed within the CRTBP model.[44] In the CRTBP, a larger body (the primary) and a smaller body (the secondary) are assumed to rotate in circular orbits about their center of mass. The motion of an infinitesimal mass is then modeled in this system. The mass ratio of the two massive bodies, referred to here collectively as the primaries, is defined to be $\mu = m_2/(m_1 + m_2)$ where m_1 is the mass of the primary and m_2 is the mass of the secondary. Mass ratios for selected systems relevant to this study are given in Table 1. The relevant quantities are then made dimensionless, and the equations of motion are formulated in a rotating frame. The rotating frame is defined with the x axis aligned along the two masses so that the primary is located at $x_1 = -\mu$ and the secondary is located at $x_2 = 1 - \mu$. The dimensionless period of the system is 2π, while the mean motion of the bodies, the distance between the primaries, and the gravitational constant are all one. The equations of motion in the rotating frame are defined with these quantities by

Table 1: Mass ratios for several selected CRTBP systems

System	μ
Sun-Earth	0.0000030404234021
Sun-Jupiter	0.0009538811803631
Earth-Moon	0.0121505842705715
Jupiter-Europa	0.0000252664488504
Saturn-Titan	0.0002365805491104

$$\ddot{x} - 2\dot{y} = \frac{\partial \Omega}{\partial x}, \quad \ddot{y} + 2\dot{x} = \frac{\partial \Omega}{\partial y}, \quad \ddot{z} = \frac{\partial \Omega}{\partial z} \tag{1}$$

where

$$\Omega = \frac{x^2 + y^2}{2} + \frac{(1-\mu)}{r_1} + \frac{\mu}{r_2} \tag{2}$$

and

$$\begin{aligned} r_1 &= \sqrt{(x - x_1)^2 + y^2 + z^2} \\ r_2 &= \sqrt{(x - x_2)^2 + y^2 + z^2}. \end{aligned} \tag{3}$$

An energy-like integral referred to as the Jacobi constant is defined by

$$C = x^2 + y^2 + \frac{2(1-\mu)}{r_1} + \frac{2\mu}{r_2} - \dot{x}^2 - \dot{y}^2 - \dot{z}^2. \tag{4}$$

For particular values of the Jacobi constant, regions known as forbidden regions where a spacecraft cannot travel are known to exist. Five equilibrium points (or Lagrange points) are known to exist, and three collinear equilibrium points are found on the x axis. L_1 is located between the primary and the secondary, and L_2 is on the far side of the secondary from the primary.

Various types of unstable periodic orbits are known to exist around the libration points including the planar Lyapunov orbits and three-dimensional halo orbits. Here Lyapunov orbits are continued for each system from an initial guess computed near the libration point of interest. Halo orbits are computed initially using Richardson and Cary's algorithm,[45] and then continued from that point using a single-shooting algorithm.[46]

Unstable orbits possess stable and unstable manifolds which provide pathways for spacecraft to travel to and from these orbits. Heuristically, the stable manifolds consist of those trajectories that approach the unstable orbit as time goes toward infinity, and the unstable manifolds are those trajectories that approach the orbit as time goes toward negative infinity. More formal definitions of the stable and unstable manifolds for a flow ϕ_t are

> Stable Manifold $W^s(L)$: Set of points x such that $\phi_t(x)$ approaches L as $t \to \infty$.
>
> Unstable Manifold $W^u(L)$: Set of points x such that $\phi_t(x)$ approaches L as $t \to -\infty$.

The stable and unstable manifolds are computed using the stability characteristics of the monodromy matrix. The offset used to compute the invariant manifolds in this

analysis was 1×10^{-6} dimensionless units. Refer to Wiggins[47] for more specific information on invariant manifolds.

The existence of certain symmetries in the CRTBP provide wider applications of the results from this study. In particular, it is known that if $(x, y, z, \dot{x}, \dot{y}, \dot{z}, t)$ is a solution in the CRTBP, then $(x, -y, z, -\dot{x}, \dot{y}, -\dot{z}, -t)$ is also a solution.[48,49] So if a trajectory is reflected about the xz plane, a valid trajectory may be found by traveling along the reflected trajectory in reverse. In other words, if an approach trajectory to a moon is computed, the departure trajectory may be found without computing a new trajectory by using this symmetry property. Although this symmetry only exists precisely in the CRTBP, it has generally been found to exist approximately in the ephemeris problem as well. See Szebehely for a more detailed description of this symmetry.

III. POINCARÉ SECTIONS

Poincaré maps have been found to be a useful tool to observe the structure of the flow and observe the relationship of the invariant manifolds of periodic orbits to one another. Anderson and Lo[26] contains a more detailed explanation of the techniques used here, while Parker and Chua,[50] and Wiggins[47] give more general explanations. To compute a Poincaré section, a hypersurface Σ, or surface of section in $\mathbb{R}^{n-1}$, is placed transverse to a flow in $\mathbb{R}^n$. The mapping is from consecutive intersections of the trajectory with Σ. The surface of section used here in the planar problem is the $y = 0$ line where $x < -\mu$. In the spatial problem, $y = 0$ gives the xz plane. A one-sided Poincaré section with $\dot{y} > 0$ is used here with constant C. For the planar case the state may be fully computed from the Poincaré section if it is plotted using x and $\dot{x}$. In this case, x, $\dot{x}$, y, and C are known, and

$$\dot{y} = \pm \sqrt{x^2 + y^2 + \frac{2(1-\mu)}{r_1} + \frac{2\mu}{r_2} - \dot{x}^2 - C}. \quad (5)$$

The integrators used to compute the Poincaré sections and the other trajectories in this study include a Runge-Kutta Fehlberg seventh-order integrator[51] with step-size control and the DIVA propagator.[52]

III.I. Ephemeris Model

The full ephemeris model was used briefly for some analyses to include multi-body effects and more closely approximate real-world trajectories. In particular, the JPL DE421 Planetary and Lunar Ephemerides were used for this study. Details on this model may be found by referring to Folkner.[53]

III.II. Resonance

One of the primary questions that is typically of interest in tour design is related to finding the last resonance that must be achieved before the final approach. In the two-body problem, the periods of the spacecraft and the secondary may be precisely related. In this case, the spacecraft may be defined to travel around the primary p times for every q times the secondary travels around the primary where $p, q \in \mathbb{N}$. The resonant integers, mean motions (n), and periods (T) may be related as

$$\frac{p}{q} = \frac{n_p}{n_q} = \frac{T_q}{T_p}. \quad (6)$$

In this paper, the form p:q is used for the resonances.

In the three-body problem, the periods at particular resonances are no longer precisely related by integers, and the definition given by Murray and Dermott for mean motion resonance may be used:

$$p n_p \approx q n_q. \quad (7)$$

See Murray and Dermott,[54] Szebehely[44], and Barrabés and Gómez[55,56] for more detailed explanations related to the theory of resonance.

In mission design, an approximation of the resonance is often computed using the two-body period of the state far from the secondary. In this study, the state is often taken at Σ on the far side of the primary from the secondary. The specific energy (E) and the semimajor axis (a) may be computed in dimensionless units as

$$E = \frac{{v_i}^2}{2} - \frac{1}{r} \quad (8)$$

and

$$a = -\frac{1}{2E} \quad (9)$$

where $r = |\mathbf{r}|$ and $v_i = |\mathbf{v_i}|$. Here, the i subscript indicates an inertial quantity. The dimensionless period of the orbit is then

$$\mathbb{P} = 2\pi \sqrt{\frac{a^3}{1}} \quad (10)$$

Normalizing by the period of the secondary around the primary, or the period of the system, gives an indication of the resonance as it is typically computed for mission design (calculated far from the secondary) as

$$\frac{\mathbb{P}}{\mathbb{P}_{sec}} = \frac{\mathbb{P}}{2\pi}. \quad (11)$$

IV. RESONANCES OF PLANAR LYAPUNOV ORBIT STABLE MANIFOLDS

In Anderson[30] Lyapunov orbits were computed for various systems over different Jacobi constants to determine the resonances that were connected to the stable manifolds of the Lyapunov orbit at the intersection with Σ. The fact that the Lyapunov orbit acts as a gateway to the secondary[57] and the trajectories approaching the secondary were contained within the Lyapunov orbit stable

manifold (W^s_{lyap}) in the Poincaré section made the analysis of the possible resonances easier. One method to compare the results from the planar analysis to this spatial analysis is to compute the two-body periods of the stable manifolds of Lyapunov and halo orbits for each case far from the secondary at Σ. The two-body period at this point has been shown to be related to the resonance in the past.[26] The periods of the trajectories may then be compared to obtain a relative understanding of the resonances that may be reached. Keep in mind that the computation of specific resonant orbits in the three-body problem is needed to determine the true resonance and more completely understand how to tie the trajectory in to the final approach. This method allows the computation of an approximate relative resonance and provides a clear distinction between interior and exterior resonances.

The approach to Europa via L_2 libration orbits in the Jupiter-Europa system is examined in detail here first, and then some analyses of the Sun-Jupiter system will be added. For this system, the family of Lyapunov orbits at L_2 may be computed over a range of Jacobi constants as shown in Figure 1. The family is shown here down to the Jacobi constant where the Lyapunov orbit just grazes the surface of Europa at $C_{graze} \approx 2.9997485$. The stable manifold trajectories of a Lyapunov orbit may

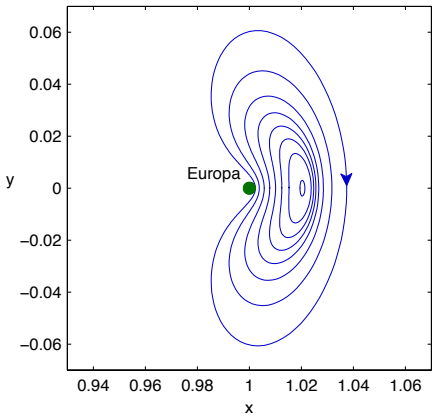

Fig. 1: Jupiter-Europa L_2 Lyapunov orbit family in the Jupiter-Europa rotating frame shown down to the orbit that grazes the surface of Europa.

be computed for a particular energy, and the intersections of these trajectories with Σ may then be determined. A plot in configuration space of the stable manifold trajectories of a Lyapunov orbit with C = 3.001 integrated out to Σ is shown in Figure 2. A Poincaré section may then be computed using the intersections of the L_2 W^s_{lyap} at Σ in x and $\dot{x}$ coordinates. The usual Poincaré section for C = 3.001 is shown in Figure 3. If the normalized two-body period is computed at Σ as described earlier, a further understanding of the relationship between the in-

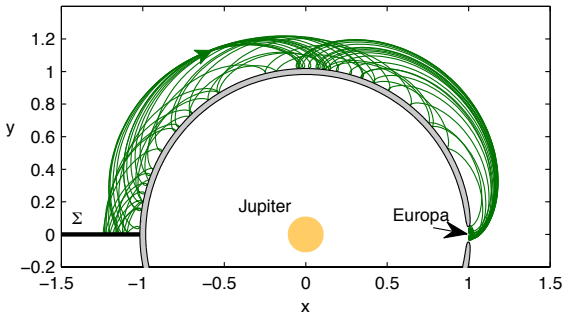

Fig. 2: W^s of a Jupiter-Europa L_2 Lyapunov orbit at C = 3.001 in the Jupiter-Europa rotating frame integrated out to the intersection with Σ.

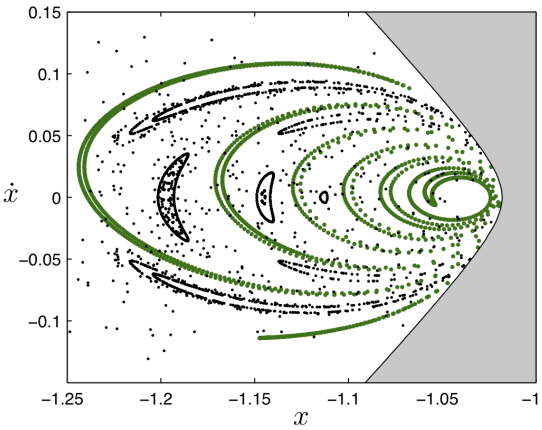

Fig. 3: Intersections of the planar L_2 W^s_{lyap} with Σ for C = 3.001.

tersections at Σ and the approximate resonance may be obtained. The plot in Figure 4 shows that the outer bands tend to have greater periods indicating that they are at a more distant resonance from Europa's orbit. This agrees with the results in Anderson[30] where particular resonant orbits at different resonances and their intersections were compared to the Lyapunov orbit stable manifolds.

One way to obtain a general understanding of the resonances that may be tied into the Lyapunov orbit is to examine the two-body period for all of the L_2 W^s_{lyap} intersections at Σ and search for the largest possible period. This process may be repeated for a range of different Lyapunov orbits over changing Jacobi constants to see the values that may be achieved. The maximum normalized periods reached by the trajectories on the stable manifold at Σ for a range of Jacobi constants in the Jupiter-Europa system are given in Figure 5. It can be seen from this plot that the periods are larger for lower Jacobi constants (higher energy) and decrease as the Lyapunov orbit size decreases. The values stay near the 5:6 resonance that was shown in Anderson and Lo[26] and Anderson[30] to be

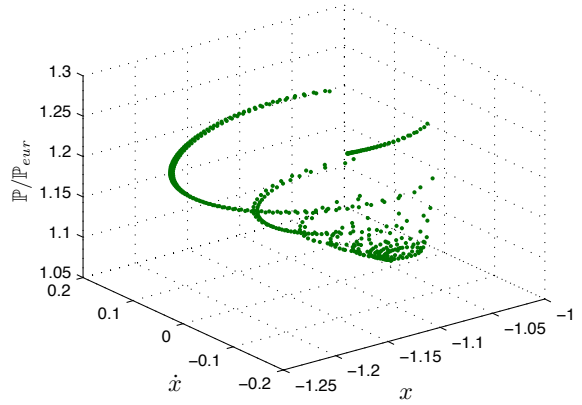

Fig. 4: Normalized periods for the planar L_2 W^s_{lyap} computed at their intersections with Σ for C = 3.001.

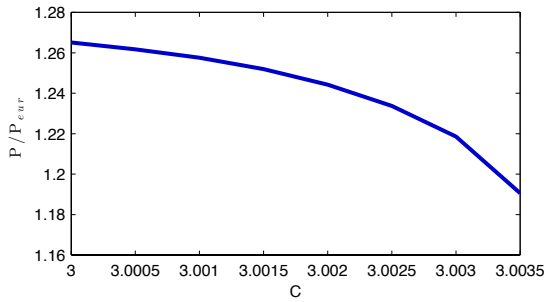

Fig. 5: Maximum normalized periods for the planar L_2 W^s_{lyap} trajectories computed at their intersections with Σ for various Jacobi constants.

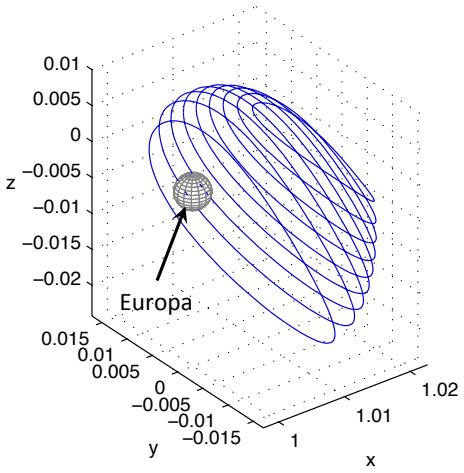

(a) Perspective View

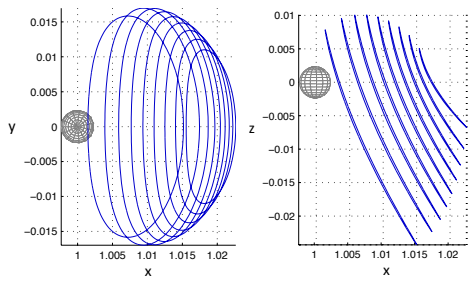

(b) *xy* view (c) *xz* view

Fig. 6: Several views of the L_2 halo orbit family in the rotating frame of the Jupiter-Europa system.

necessary in the resonant sequence for the final approach at the energies of interest.

V. COMPARISON OF HALO AND LYAPUNOV ORBIT STABLE MANIFOLDS AT Σ

One starting place to examine the spatial version of the problem is to examine the L_2 halo orbits and their invariant manifolds. The halo orbit family for a range of Jacobi constants is shown in Figure 6. It is immediately apparent that the halo orbits are generally smaller in size than the Lyapunov orbits, but they have the potential to provide the three-dimensional approach desired for many mission scenarios. A process similar to that used with the planar Lyapunov orbits may now be used with the halo orbits to compute intersections with Σ where Σ is now the *xz* plane. The computed periods give additional insight into the resonances reached by the spacecraft since the Poincaré sections no longer represent the complete state of the trajectory. The trajectories are still relatively near the plane, and the normalized periods at these intersections may be computed for comparison with the periods achieved in the planar case. This process was completed for a range of Jacobi constants from 3.001 to 3.003, and the resulting normalized periods ranged from approximately 1.201 to 1.207 at the higher Jacobi contants. So the spatial halo orbits cover a smaller range of periods for similar Jacobi constants than the Lyapunov orbits. This result can be examined in more detail by comparing the Poincaré sections of the different cases. For the spatial problem, the complete state may no longer be obtained from the Poincaré sections. However, the plots can provide some insight into this result.

The Poincaré sections for two additional Jacobi constants are shown for comparison in Figure 7 for the planar problem. In these cases, as the arms of the stable manifolds of the Lyapunov orbit reach further to the left, the maximum period obtained increases, and the characteristics of the bands changes significantly with the Jacobi constant.

If the halo orbit W^s is integrated out to Σ as shown in Figure 8, the evolution of the halo orbit can be seen with Jacobi constant. These trajectories are three-dimensional but still relatively close to the plane. It can be seen that although the characteristics of the stable manifolds are

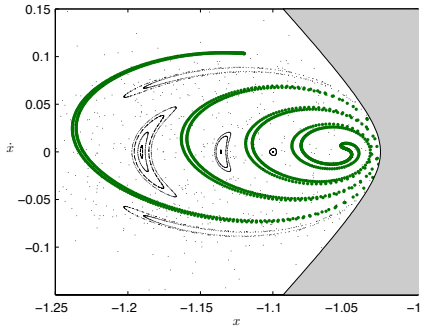

(a) C = 3.002, Max. $\mathbb{P}/\mathbb{P}_{sec} \approx 1.244$

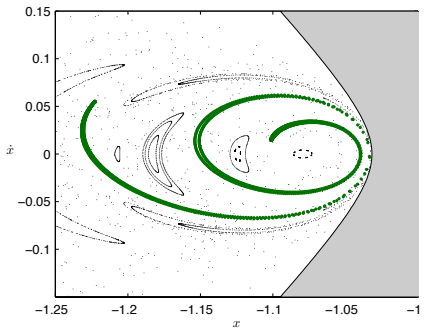

(b) C = 3.003, Max. $\mathbb{P}/\mathbb{P}_{sec} \approx 1.218$

Fig. 7: Poincaré section containing intersections of the L_2 W^s_{lyap} at Σ in the Jupiter-Europa planar problem.

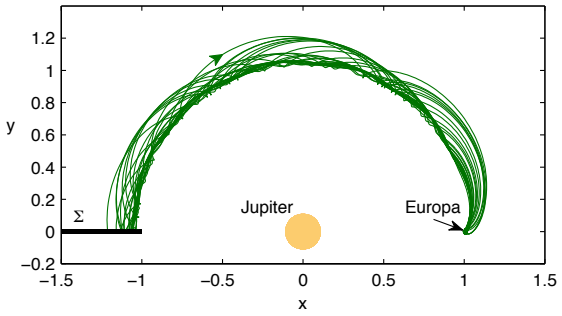

(a) C = 3.001

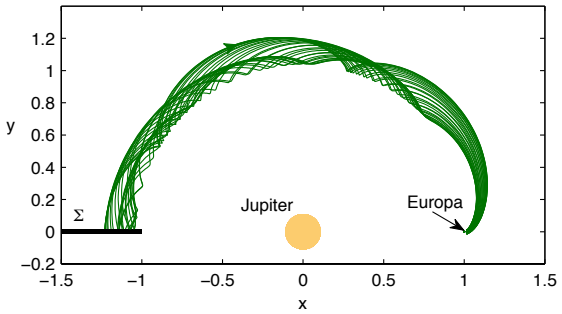

(b) C = 3.003

Fig. 8: Halo orbit L_2 W^s stable manifold trajectories projected into the *xy* plane.

changing, the location of the intersections with Σ are similar for the different Jacobi constants. Examining the halo orbit Poincaré sections in Figure 9 confirms that the left-most band in each figure does not vary significantly with the Jacobi constant, while the inner bands change more noticeably. Again, the complete state is not represented in these plots for the spatial problem, but the results line up with the observed change in the periods with Jacobi constant.

VI. PLANAR COMPARISON OF RESONANCE AND INVARIANT MANIFOLDS

While the location of the manifold intersections in Σ is useful to help understand the resonances that may be achieved, another technique examining trajectories at the surface integrated backward in time has been found to be helpful. An initial analysis of this problem was undertaken using the concept of collision orbits in Anderson and Lo.[41] Here collision orbits intersecting the surface of Europa were integrated backward in time, and the normalized period was computed at this later time. The origins of the trajectories were then categorized in a broad sense. A similar idea was used to summarize the origin of various trajectories in Von Kirchbach et al. [40] and Anderson and Parker[43,58] as compared to the invariant manifolds of libration orbits. In this study, rather than integrating backward to one of the primaries, the trajectories are integrated to Σ, and the normalized period of the trajectories is examined within the context of the invariant manifolds of libration orbits. This process is most clearly and generally done within the planar problem where a two-dimensional plot may be used to capture the relevant information, so the process is illustrated here for selected cases in the planar problem. In each case, the trajectories are represented by a plot over the surface, and the state of the trajectory is parameterized for a given C using α and θ as shown in Figure 10. A similar technique will then be used within the spatial problem to compare the general approach trajectories to the invariant manifolds of halo orbits.

It is interesting to examine a case a little less than the point at which the forbidden regions cut off transport between Europa and the interior and exterior regions. The unstable manifolds of the L_1 and L_2 Lyapunov orbits computed for a Jacobi constant of C = 3.0035 are shown in Figure 11(a). Any intersections with Europa are searched for over a period of 10 dimensionless time units, and all of the unstable manifold trajectories that intersect Europa over this time period are plotted in the figure. It can be seen from this plot that there is an initial set of direct intersections of the unstable manifold trajectories and a subsequent set of intersections after the trajectories

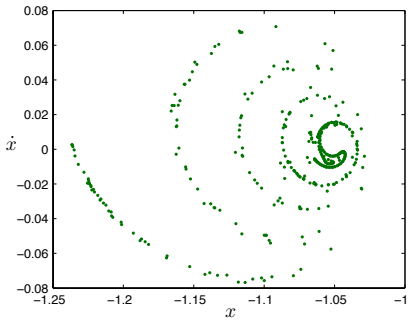

(a) C = 3.001, Max. $\mathbb{P}/\mathbb{P}_{sec} \approx 1.201$

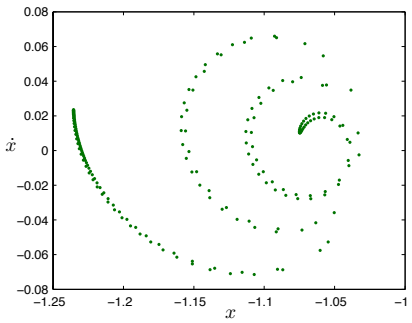

(b) C = 3.002, Max. $\mathbb{P}/\mathbb{P}_{sec} \approx 1.207$

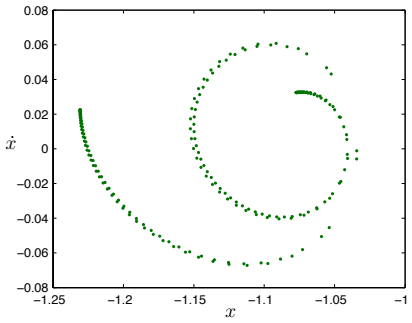

(c) C = 3.003, Max. $\mathbb{P}/\mathbb{P}_{sec} \approx 1.207$

Fig. 9: Poincaré section containing intersections of the L_2 halo orbit W^s at Σ in the Jupiter-Europa system. Remember that for this spatial case, the complete state can not be obtained from the plot.

travel through another apoapse relative to Europa. The plots will of course vary depending on the duration of the integration of the invariant manifolds. The duration times chosen for trajectory integrations in this paper have been chosen heuristically to most clearly show the structures of interest. The time of flight values typical for the final approach have also been considered. If the intersections with the surface are plotted as shown in Figure 11(b), it is found that the unstable manifolds intersect the surface along particular curves. The invariant manifolds bound distinct regions in this case, and these regions can be examined in more detail by looking at the set of trajectories leaving the surface and comparing them to the invariant manifolds. To make this comparison, trajectories encountering the surface at each point were integrated backward in time for all values of θ. As this portion of the study is geared more to looking at an approach from an exterior resonance, the maximum resonance obtained for all trajectories intersecting Σ was then computed for each point on the surface. The results are plotted in Figure 11(c) for comparison with the unstable manifold intersections of the L_1 and L_2 Lyapunov orbits. It is immediately apparent that the unstable manifolds bound the type of motion or origins of the trajectories traveling toward the surface of Europa. Those trajectories enclosed within the unstable manifold intersections of the L_1 orbit travel backward in time toward the interior region, and those enclosed within the L_2 intersections travel toward the exterior region. The maximum period obtained in this case is approximately the same upper period as that obtained by the stable manifold of the L_2 Lyapunov orbit at this same energy in Figure 5. This result indicates that the invariant manifolds can be used to find the bounds of the possible approximate resonances of trajectories traveling toward the surface as a function of the Jacobi constant. These results also show how the trajectories pass through the L_1 and L_2 gateways described by Conley.[57] The plot in Figure 11(c) provides a visual method of determining the states on the surface of the secondary that may be reached from various resonances or periods obtained just prior to the final approach.

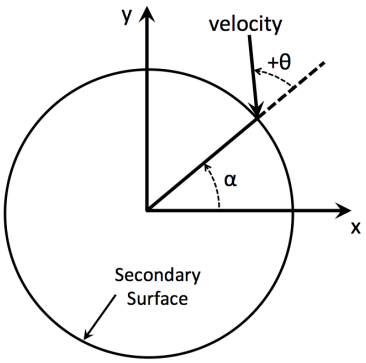

Fig. 10: Angles used to describe the state of a trajectory as it intersects the surface of the secondary. α specifies the location of the intersection on the surface of the secondary, and θ indicates the angle of the velocity relative to the surface.

The same procedure may now be repeated for various Jacobi constants to determine the possible approaches via invariant manifolds of the trajectories approaching Europa along the invariant manifolds. Plots of the invariant manifolds compared to the other approach trajectories for

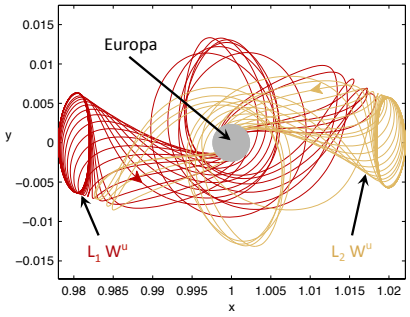

(a) Jupiter-Europa L_1 and L_2 Lyapunov orbit unstable manifold trajectories that intersect the surface of Europa.

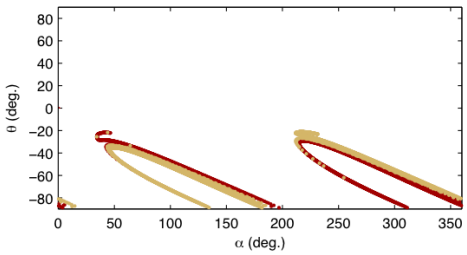

(b) Intersections of the L_1 and L_2 Lyapunov orbit unstable manifold trajectories with Europa

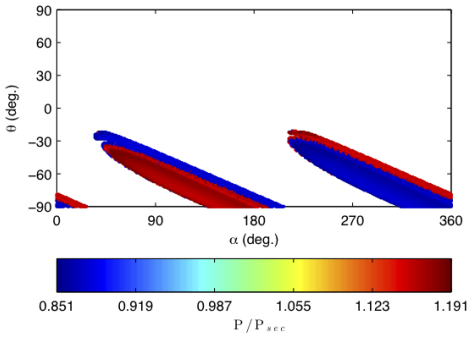

(c) Normalized Periods at Σ

Fig. 11: Comparison of Jupiter-Europa L_1 and L_2 W^u_{lyap} trajectories to general approach trajectories at C = 3.0035.

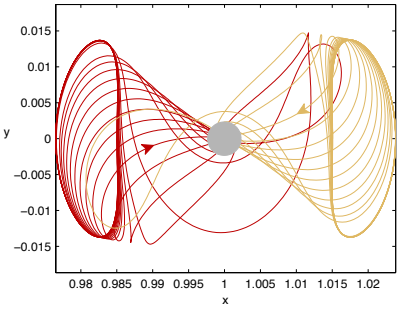

(a) Jupiter-Europa L_1 and L_2 Lyapunov orbit unstable manifold trajectories that intersect the surface of Europa.

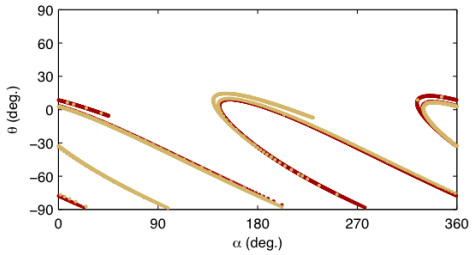

(b) Intersections of the L_1 and L_2 Lyapunov orbit unstable manifold trajectories with Europa

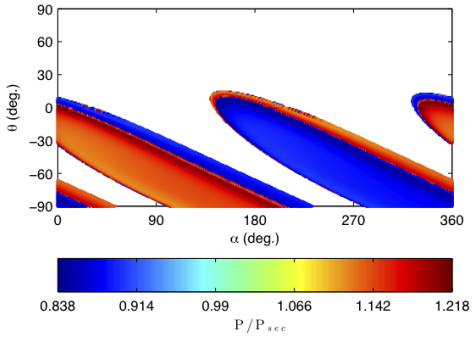

(c) Normalized Periods at Σ

Fig. 12: Comparison of Jupiter-Europa L_1 and L_2 W^u_{lyap} trajectories to general approach trajectories at C = 3.003.

a lower Jacobi constant of C = 3.003 are shown in Figure 12. In these plots, it can be seen that the Lyapunov orbits have increased in size, and the intersections with the surface of Europa have grown to enclose a larger area. The intersections of the trajectories computed for varying α and θ show the same relationship to the invariant manifolds as seen for C = 3.0035. The relationship between the invariant manifolds and the approach trajectories may be more easily seen by examining the enlarged views of the intersections in Figure 13. Here, the narrow band of trajectories originating in the exterior region is clearly enclosed in the L_2 W^u_{lyap} intersections, while the larger set of trajectories traveling to the interior region is bounded by the L_1 W^u_{lyap} intersections. The situation is reversed for the other band of exterior/interior origin trajectories. As C decreases further to C = 3.001 as shown in Figure 14, the invariant manifold intersections form bands across the plot. As would be expected for a lower C (higher energy), more options exist for approaching the surface, and the maximum periods of the trajectories approaching the surface match the values anticipated from the Lyapunov orbit bounds computed earlier.

The same procedure may also be repeated for different systems to determine how the approach scenario might vary for these systems. The output for the Sun-Jupiter

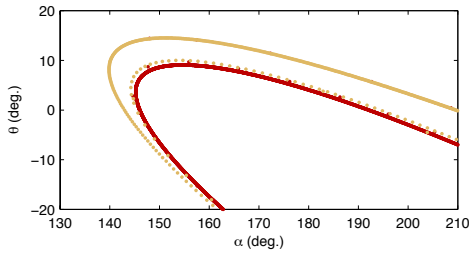

(a) Intersections of the L_1 and L_2 Lyapunov orbit unstable manifold trajectories with Europa

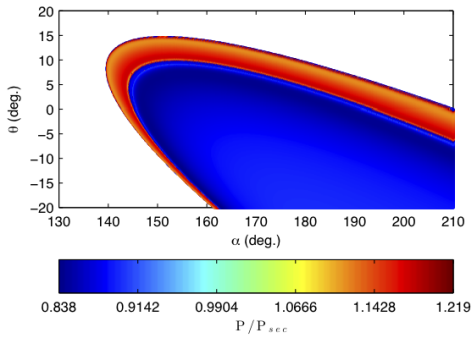

(b) Normalized Periods at Σ

Fig. 13: Closer view of comparison in Figure 12

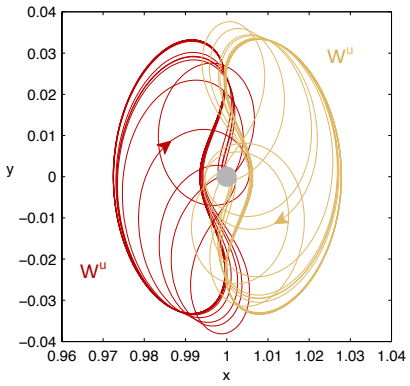

(a) Jupiter-Europa L_1 and L_2 Lyapunov orbit unstable manifold trajectories that intersect the surface of Europa

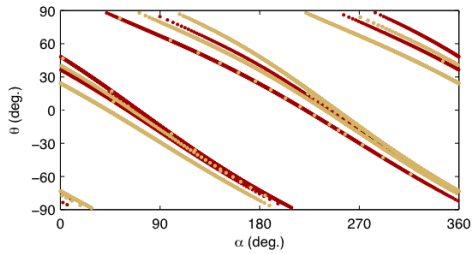

(b) Intersections of the L_1 and L_2 Lyapunov orbit unstable manifold trajectories with Europa

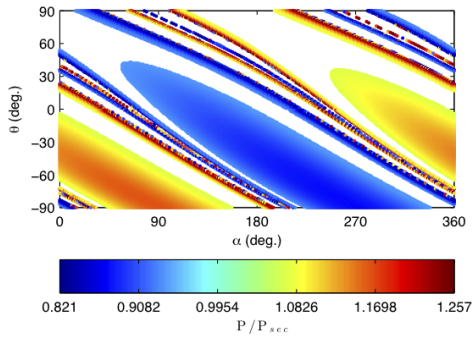

(c) Normalized Periods at Σ

Fig. 14: Comparison of Jupiter-Europa L_1 and L_2 W^u_{lyap} trajectories to general approach trajectories at C = 3.001.

system for C = 3.035 is shown in Figure 15. In this system, the Lyapunov orbits are relatively large compared to the secondary than in the Jupiter-Europa system. A greater variety of bands of trajectory types is observed in Figure 15(c) when compared to similar plots in the Jupiter-Europa system, but the overal characteristics are the same. Additional sets of intersections of the W^u_{lyap} with the surface can be observed for this integration time period when the invariant manifolds in 15(b) are examined. In each case, the same type of bounding behavior of the trajectories is observed.

VII. SPATIAL APPROACHES COMPARED TO THE INVARIANT MANIFOLDS AT Σ

For spatial approaches, the basic question is how are approaches intersecting the surface at all angles related to the invariant manifolds of libration orbits? One way to obtain a general understanding of this relationship is to compare the intersections of the general approach trajectories and the invariant manifolds of libration orbits at Σ to search for any significant differences. A plot of the invariant manifold intersections in Figure 16(a) for a Jacobi constant of C = 3.001 may be compared to the intersecting trajectories in Figure 16(b). Here, the trajectories shown in Figure 16(b) are generated at a single point with varying azimuth and elevation angles to allow the structure to be shown. It can be seen from these plots that the combined invariant manifolds of the Lyapunov and halo orbits at this energy provide a good approximation of the intersections that will be obtained by the trajectories encountering Europa, especially in the outer loop. The strict boundary seen in the planar problem with Lyapunov orbits[30] no longer exists because three-dimensional trajectories are now included. Many of the trajectories line up with the Lyapunov orbit stable manifolds, with some of them falling outside the invariant manifold boundary just as the halo orbit invariant manifolds do. A sample of results from the ephemeris problem corresponding to

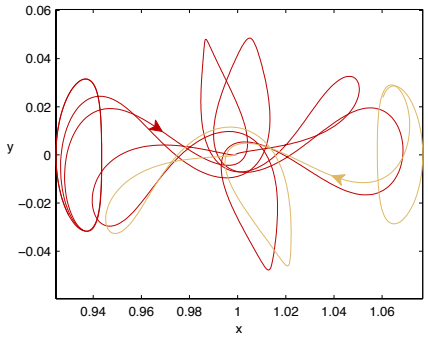

(a) Sun-Jupiter L_1 and L_2 Lyapunov orbit unstable manifold trajectories that intersect the surface of Jupiter

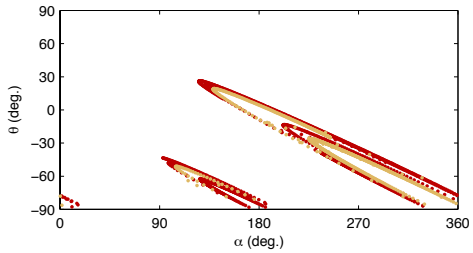

(b) Intersections of the L_1 and L_2 Lyapunov orbit unstable manifold trajectories with Jupiter

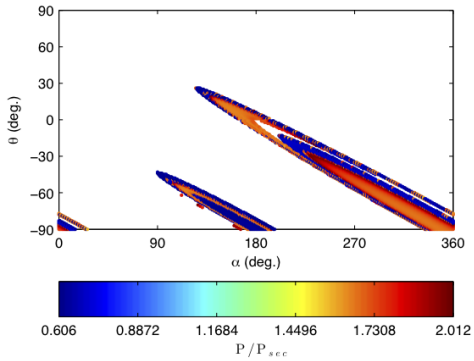

(c) Normalized Periods at Σ

Fig. 15: Comparison of Sun-Jupiter L_1 and L_2 W^u_{lyap} trajectories to general approach trajectories at C = 3.035.

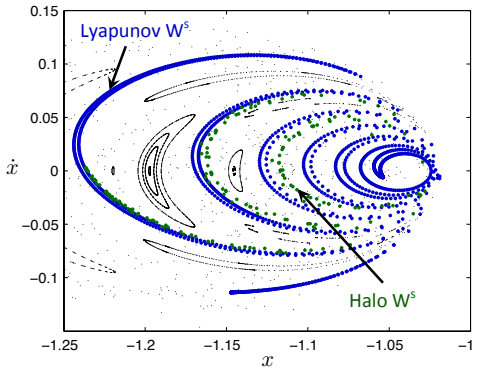

(a) L_2 Lyapunov and halo orbit stable manifold intersections

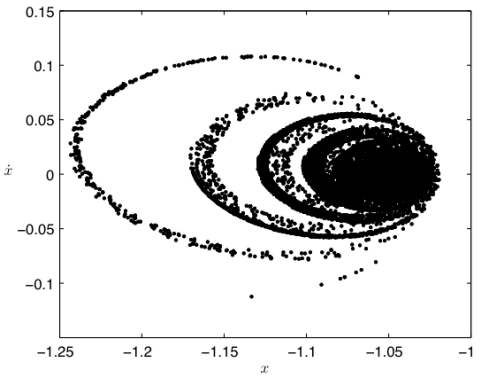

(b) Intersection of points integrated from $(\alpha,\beta) = (0°, 0°)$ with Σ in the CRTBP

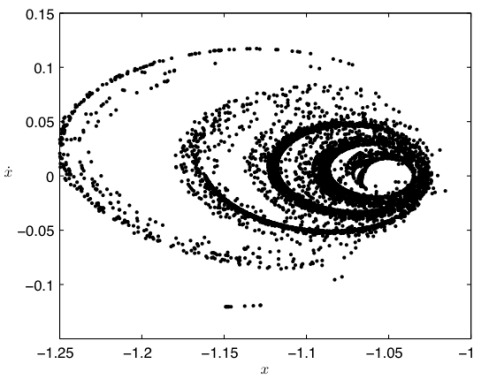

(c) Intersection of points integrated from $(\alpha,\beta) = (0°, 0°)$ with Σ in the ephemeris model

Fig. 16: General comparison of points integrated from the surface of Europa to the stable manifold intersections of libration orbits at Σ.

the CRTBP results in Figure 16(b) are shown in Figure 16(c). To save space here this information will be analyzed in more detail in a future paper, but the ephemeris results generally match those in the CRTBP with some variations similar to those shown here that also depend on the epoch of integration. This technique provides an overview of the types of resonances that are possible, but it is useful to turn to other techniques for more specific information.

VIII. RESONANCE AT THE SURFACE

A general overview of the types of periods or resonances that may be achieved in the spatial problem may be obtained by computing the periods at Σ of trajectories encountering different points on the secondary's surface

approaching from various azimuth and elevation angles. This computation was performed over the surface of Europa for various Jacobi constant values, and the maximum periods that were achieved are plotted in Figure 17. In this plot, α is the same as described in Figure 10 and β is measured like latitude above the xy plane of the rotating frame. Points were plotted using 1 degree increments in α and β. Azimuth is defined with North at 0° and elevation is measured positive above the surface. Azimuth was varied in increments of 10 degrees, while the elevation was varied in 3 degree increments. An integration time interval of 45 dimensionless units was chosen based on past experience. The maximum periods obtained for

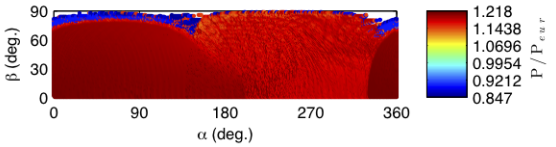

(a) C = 3.003, Max. $\mathbb{P}/\mathbb{P}_{sec} \approx 1.218$

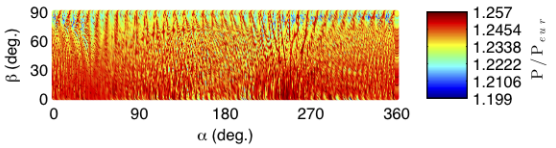

(b) C = 3.001, Max. $\mathbb{P}/\mathbb{P}_{sec} \approx 1.257$

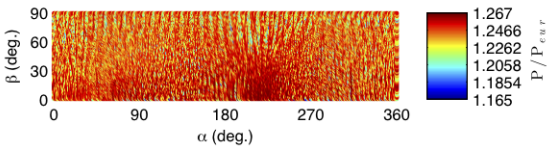

(c) C = $C_{graze} \approx 2.9997485$, Max. $\mathbb{P}/\mathbb{P}_{sec} \approx 1.267$

Fig. 17: Maximum resonance obtained for all trajectories computed at different azimuth and elevation angles at each point on the surface. (Jupiter-Europa system)

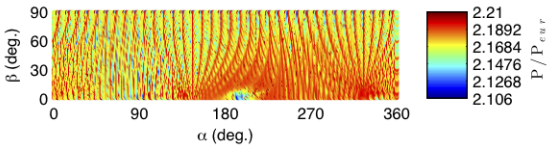

Fig. 18: Maximum resonance obtained for all trajectories computed at different azimuth and elevation angles at each point on the surface. C = 3.03, Max. $\mathbb{P}/\mathbb{P}_{sec} \approx 2.21$, Sun-Jupiter system.

each Jacobi constant line up well with the maximum periods obtained using the Lyapunov orbit stable manifolds indicating again that the Lyapunov orbit stable manifolds serve as an excellent guide for the general types of resonances that are possible for each Jacobi constant. For C = 3.003, it can be seen that the periods are generally smaller, and some of the points at the higher latitudes do not reach exterior resonances for this integration time period. A sample of results from the Sun-Jupiter system are given in Figure 18. Similar overall trends are observed for this system although the differences in each region are generally more distinct.

IX. FINAL SPATIAL APPROACH COMPARED TO INVARIANT MANIFOLDS

It is clear that the periods obtained by trajectories approaching the surface are related to the invariant manifolds of libration point orbits in a general sense of the periods that are obtainable, and the invariant manifolds of the Lyapunov orbits in the planar problem provide a clear division in the origins of various trajectories. Now the relationship between the final segment of the approach and the invariant manifolds of halo orbits in the spatial problem will be analyzed. This relationship may first be examined by simply plotting the usual unstable manifolds of a halo orbit and computing their intersections with the secondary. A set of trajectories on the unstable manifold of an L_2 halo orbit are computed for the Jupiter-Europa system at C = 3.003, and the trajectories that impact the surface of Europa are shown in Figures 19 and 20. Here,

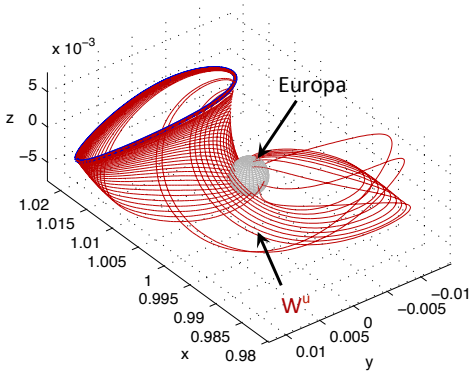

Fig. 19: L_2 halo orbit W^u with its intersections at Europa for C = 3.003.

the length of time of the integration becomes a factor in the trajectories that are shown. As we are interested only in those trajectories with the most direct approach, the integration time was limited to less than 4π dimensionless time units. It is apparent from the plot that for this Jacobi constant and integration time, there are two distinct sets of intersections. The first set of intersections occurs more directly, and a second set swings past Europa and intersects after traveling through another apoapse. The color in the intersection points plotted in Figure 21 corresponds to integration time with lighter colors indicating a later time. It can be seen that the majority of the inter-

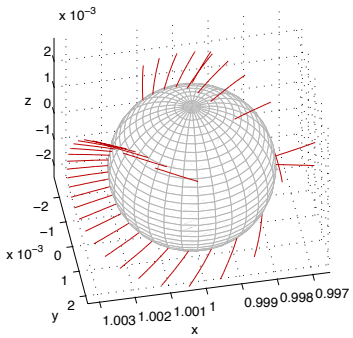

Fig. 20: Closer view of the intersections in Figure 19

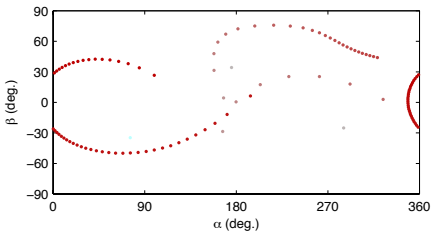

Fig. 21: Intersections of the halo orbit W^u in Figure 19 plotted on the surface of Europa where the lighter points intersect Europa at later times.

sections at this Jacobi constant occur in the large curve around the 0° β line.

Although the location of the invariant manifold intersections are useful, the orientation of the approach is often needed for mission design constraints. This information is plotted in Figure 22 where the locations are indicated by the symbols, and the orientation of the intersection with the surface is given by a combination of the orientation of the line attached to the symbol (azimuth) and the color of the line (elevation). A sample of the results for several different Jacobi constants are shown in the figure to provide an idea of how the intersections vary over energy. Similar results exist for other systems, and they will be given in a future paper where the full results can be presented.

While the plot in Figure 22 provides useful information, understanding how the more direct trajectories approach the secondary and how they are related to these invariant manifolds is key to the mission design problem. Insight into this question may be gained by examining the approach of trajectories to the surface at particular intersections of the unstable manifold trajectories with the surface of Europa. This comparison is performed by selecting a particular intersection of the L_2 halo orbit W^u with the surface and then integrating a set of trajectories backward in time using different azimuth and elevation angles. The trajectories are integrated for 45 dimensionless time units, and the periods of any trajectories that

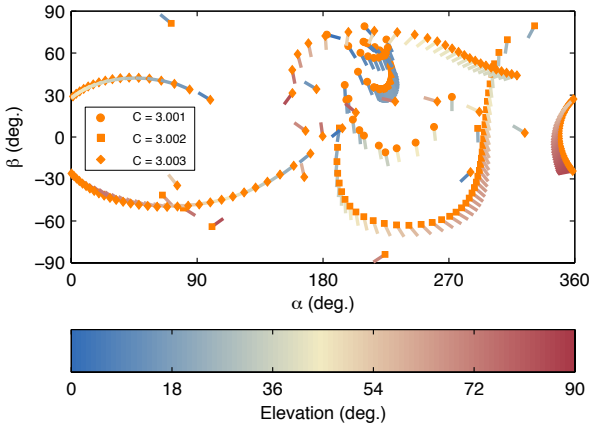

Fig. 22: Intersections of halo orbit W^u including the orientation of the encounter for selected Jacobi constants.

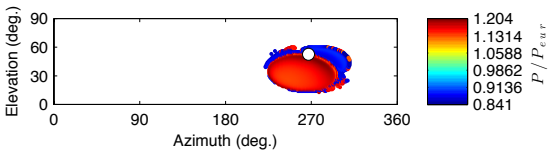

(a) $\alpha \approx 91.4^o, \beta \approx$ -48.2^o

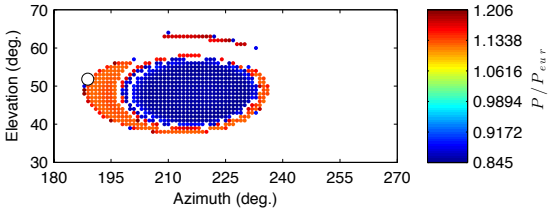

(b) $\alpha \approx 198.2^o, \beta \approx 75.2^o$

Fig. 23: Comparisons of two halo orbit W^u trajectory intersections with other trajectories approaching the surface at C = 3.003

intersect Σ within this time interval are computed and plotted as shown in Figure 23. Here, the normalized periods of each trajectory integrated backward in time are plotted for each combination of azimuth and elevation, and the intersection of the unstable manifold is indicated by a white point. A close relationship is seen between the invariant manifolds and the trajectories in that the unstable manifold intersection in Figure 23(a) lies on the boundary between those trajectories traveling to exterior and interior resonances. Also, for this energy, the majority of azimuth and elevation angles do not reach Σ, but the relatively small area of trajectories that do are all near the invariant manifold intersection. This result provides a potential pathway for further understanding the possible approaches at a particular location and deserves further exploration. A general relationship between trajectories traveling to the Earth and Moon and invariant manifolds

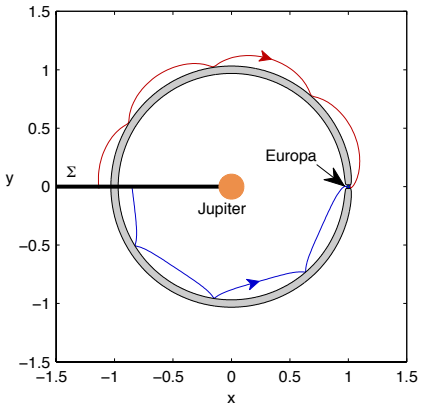

(a) Overview

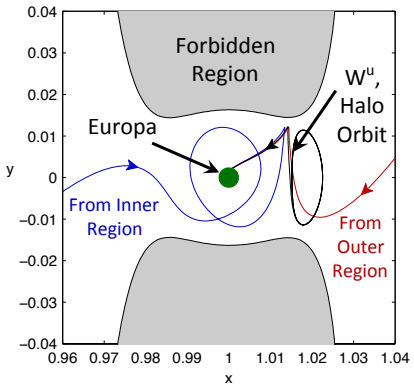

(b) Region Near Europa

Fig. 24: Comparison of the W^u trajectory corresponding to the intersection in Figure 23(a) to nearby trajectories originating in the inner and outer regions. The spatial trajectories have been projected into the *xy* plane.

in the Earth-Moon system was observed in Anderson and Parker,[43] but these results clearly show a relationship between the invariant manifolds and the dividing line between the trajectories traveling to the exterior or interior regions. A closer view of the results from another intersection of the unstable manifold is shown in Figure 23(b), and the intersection again lies on a boundary. If the unstable manifold intersection and nearby trajectories going to the interior and exterior regions are plotted as shown in Figure 24, the behavior of the trajectories near this region may be more clearly observed. The unstable manifold acts as a divider between the behavior of the trajectories. One trajectory follows the invariant manifold trajectory and travels backward in time through the gateway to the exterior region. The other trajectory falls back from the L_2 gateway and travels to the interior region. The trajectory that follows the unstable manifold in from the exterior region but avoids winding onto the halo orbit would potentially be useful for mission design scenarios. The plot confirms that there are trajectories near the invariant manifolds that possess similar characteristics that could avoid asympototic approaches and reduce transfer time requirements.

X. CONCLUSION

A variety of techniques were developed to compare spatial approaches to moons with the invariant manifolds of Lyapunov and halo orbits, and they were applied to cases in the Jupiter-Europa and Sun-Jupiter systems. The possible two-body periods or approximate resonances reachable by the stable manifolds of the L_2 Lyapunov orbits just prior to the final approach were found to provide an upper bound on the approximate resonances for spatial trajectories before they approached the moon. This was verified for the Jupiter-Europa system over Jacobi constants ranging from 3.001 to 3.003. It was shown that the invariant manifolds of the Lyapunov orbits in the planar problem provide a clear boundary between trajectories approaching the surface of the moon from exterior and interior resonances. Spatial halo orbit invariant manifold intersections were also found to lie on the boundaries of orbits originating from the exterior and interior resonances. The invariant manifolds of libration orbits were found to serve as a useful guide for the approach problem in the analyzed cases including determining the possible approximate resonances before final approach and during the last portion of the approach phase.

XI. FUTURE WORK

The comparison techniques will be further developed and applied to new cases in additional systems to explore the problem more generally. Further work will focus on moving beyond the two-body approximations to more accurately determine the resonances. Spatial resonant orbits will be developed to aid in this process, and techniques for tying in the last portion of the tour to this final approach will be studied. Additional work will include expanding the analysis to other types of periodic orbits. Ephemeris effects will be incorporated, especially for specific mission design scenarios.

XII. ACKNOWLEDGEMENTS

The authors would like to thank Jon Sims and Damon Landau for their helpful comments and careful reviews of this paper. The research presented in this paper has been carried out at the Jet Propulsion Laboratory, California Institute of Technology, under a contract with the National Aeronautics and Space Administration.

XIII. REFERENCES

[1] J. A. Sims, J. M. Longuski, Analysis of V_∞ Leveraging for Interplanetary Missions, AIAA/AAS Astrodynamics Conference, AIAA-1994-3769, Scottsdale, AZ, 1994.

[2] S. Campagnola, R. Russell, Endgame Problem Part 1: V-Infinity-Leveraging Technique and the Leveraging Graph, Journal of Guidance, Control, and Dynamics 33 (2) (2010) 463–475.

[3] R. C. Woolley, D. J. Scheeres, Hyperbolic Periodic Orbits in the Three-Body Problem and their Application to Orbital Capture, AAS George H. Born Symposium, Boulder, CO, 2010.

[4] G. J. Whiffen, Mystic: Implementation of the Static Dynamic Optimal Control Algorithm for High Fidelity Low Thrust Trajectory Design, AIAA/AAS Astrodynamics Specialists Conference, AIAA-2006-6741, Keystone, CO, 2006.

[5] G. J. Whiffen, T. Lam, The Jupiter Icy Moons Orbiter Reference Trajectory, AAS/AIAA Space-Flight Mechanics Meeting, AAS 06-186, Tampa, FL, 2006.

[6] G. Lantoine, R. P. Russell, S. Campagnola, Optimization of Low-Energy Resonant Hopping Transfer Between Planetary Moons, 60th IAC, IAC-09.C1.1.1, Deajeon, Korea, 2010.

[7] G. Lantoine, R. P. Russell, Near-Ballistic Halo-to-Halo Transfers Between Planetary Moons, AAS George H. Born Astrodynamics Symposium, Boulder, CO, 2010.

[8] E. Bollt, J. D. Meiss, Targeting Chaotic Orbits to the Moon through Recurrence, Physics Letters A 204 (1995) 373–378.

[9] C. G. Schroer, E. Ott, Targeting in Hamiltonian Systems that have Mixed Regular/Chaotic Phase Spaces, Chaos 7 (4) (1997) 512–519.

[10] E. Belbruno, B. Marsden, Resonance Hopping in Comets, Astronomical J. 113 (1997) 1433–1444.

[11] M. Lo, S. Ross, Low Energy Interplanetary Transfers Using Invariant Manifolds of L1, L2, and Halo Orbits, AAS/AIAA Space Flight Mechanics Meeting, AAS 98-136, Monterey, CA, 1998.

[12] M. Okutsu, T. J. Debban, J. M. Longuski, Tour Design Strategies for the Europa Orbiter Mission, AAS/AIAA Astrodynamics Specialist Conference, AAS 01-463, 2001.

[13] N. J. Strange, J. M. Longuski, Graphical Method for Gravity-Assist Trajectory Design, Journal of Spacecraft and Rockets 39 (1) (2002) 9–16.

[14] S. Campagnola, R. Russell, Endgame Problem Part 2: Multibody Technique and the Tisserand-Poincare Graph, Journal of Guidance, Control, and Dynamics 33 (2) (2010) 476–486.

[15] K. W. Kloster, A. E. Petropoulos, J. M. Longuski, Europa Orbiter Tour Design with Io Gravity Assists, Acta Astronautica 68 (2010) 931–946.

[16] S. D. Ross, D. J. Scheeres, Multiple Gravity Assists, Capture, and Escape in the Restricted Three-Body Problem, Siam Journal On Applied Dynamical Systems 6 (2007) 576–596.

[17] E. S. Gawlik, J. E. Marsden, S. Campagnola, A. Moore, Invariant Manifolds, Discrete Mechanics, and Trajectory Design for a Mission to Titan, 19th AAS/AIAA Space Flight Mechanics Meeting, AAS 09-226, Savannah, GA, 2009, pp. 1887–1903.

[18] W. S. Koon, M. W. Lo, J. E. Marsden, S. D. Ross, Heteroclinic Connections between Periodic Orbits and Resonance Transitions in Celestial Mechanics, Chaos 10 (2) (2000) 427–469.

[19] W. S. Koon, M. W. Lo, J. E. Marsden, S. D. Ross, Resonance and Capture of Jupiter Comets, Celestial Mechanics 81 (1-2) (2001) 27–38.

[20] K. C. Howell, B. Marchand, M. W. Lo, Temporary Satellite Capture of Short-Period Jupiter Family Comets from the Perspective of Dynamical Systems, J. of the Astronautical Sciences 49 (4) (2001) 539–557.

[21] M. W. Lo, R. L. Anderson, G. Whiffen, L. Romans, The Role of Invariant Manifolds in Low Thrust Trajectory Design (Part I), AAS/AIAA Spaceflight Dynamics Conference, AAS 04-288, Maui, HI, 2004.

[22] R. L. Anderson, M. W. Lo, The Role of Invariant Manifolds in Low Thrust Trajectory Design (II), AIAA/AAS Astrodynamics Specialist Conference, AIAA 2004-5305, Providence, RI, 2004.

[23] R. L. Anderson, Low Thrust Trajectory Design for Resonant Flybys and Captures Using Invariant Manifolds, Ph.D. thesis, University of Colorado at Boulder, http://ccar.colorado.edu/~rla/papers/andersonphd.pdf (2005).

[24] M. W. Lo, R. L. Anderson, T. Lam, G. Whiffen, The Role of Invariant Manifolds in Low Thrust Trajectory Design (III), AAS/AIAA Astrodynamics Specialist Conference, AAS 06-190, Tampa, FL, 2006.

[25] R. L. Anderson, M. W. Lo, Role of Invariant Manifolds in Low-Thrust Trajectory Design, Journal of Guidance, Control, and Dynamics 32 (6) (2009) 1921–1930.

[26] R. L. Anderson, M. W. Lo, Dynamical Systems Analysis of Planetary Flybys and Approach: Planar Europa Orbiter, Journal of Guidance, Control, and Dynamics 33 (6) (2010) 1899–1912.

[27] R. L. Anderson, M. W. Lo, Flyby Design using Heteroclinic and Homoclinic Connections of Unstable Resonant Orbits, AAS/AIAA Space Flight Mechanics Meeting, AAS 11-125, New Orleans, LA, 2011.

[28] M. Vaquero, K. C. Howell, Poincaré Maps and Resonant Orbits in the Circular Restricted Three-Body Problem, AAS/AIAA Astrodynamics Specialist Conference, AAS 11-428, AK, 2011.

[29] R. L. Anderson, M. W. Lo, A Dynamical Systems Analysis of Planetary Flybys and Approach: Bal-

listic Case, J. of the Astronautical Sciences 58 (2) (2011) 167–194.
[30] R. L. Anderson, Approaching Moons from Resonance via Invariant Manifolds, 22nd AAS/AIAA Space Flight Mechanics Meeting, AAS 12-136, Charleston, SC, 2012.
[31] P. A. Finlayson, PTool Version 1.0 Documentation, Tech. Rep. Jet Propulsion Laboratory (July 1999).
[32] T. Sweetser, R. Maddock, J. Johannesen, J. Bell, P. Penzo, A. Wolf, S. Williams, S. Matousek, S. Weinstein, Trajectory Design for a Europa Orbiter Mission: A Plethora of Astrodynamic Challenges, AAS/AIAA Spaceflight Mechanics Meeting, AAS 97-174, Huntsville, AL, 1997.
[33] J. R. Johannesen, L. A. D'Amario, Europa Orbiter Mission Trajectory Design, AAS/AIAA Astrodynamics Specialist Conference, AAS 99-360, Girdwood, AK, 1999.
[34] D. J. Grebow, A. E. Petropoulos, P. A. Finlayson, Multi-Body Capture to Low-Altitude Circular Orbits at Europa, AAS/AIAA Astrodynamics Specialist Conference, AAS 11-427, Girdwood, AK, 2011.
[35] M. W. Lo, The Interplanetary Superhighway and the Origins Program, Aerospace Conference Proceedings (2002), IEEE, Vol. 7, 2001, pp. 3543–3562.
[36] W. S. Koon, M. W. Lo, J. E. Marsden, S. D. Ross, Constructing a Low Energy Transfer Between Jovian Moons, Celestial Mechanics, 2002, pp. 129–146.
[37] F. Topputo, M. Vasile, F. Bernelli-Zazzera, Low Energy Interplanetary Transfers Exploiting Invariant Manifolds of the Restricted Three-Body Problem, J. of the Astronautical Sciences 53 (4) (2005) 353–372.
[38] G. Lantoine, A Methodology for Robust Optimization of Low-Thrust Trajectories in Multi-Body Environments, Ph.D. thesis, Georgia Tech., Atlanta, GA (2010).
[39] B. F. Villac, D. J. Scheeres, Escaping Trajectories in the Hill Three-Body Problem and Applications, Journal of Guidance, Control, and Dynamics 26 (2) (2003) 224–232.
[40] C. von Kirchbach, H. Zheng, J. Aristoff, J. Kavanagh, B. F. Villac, M. W. Lo, Trajectories Leaving a Sphere in the Restricted Three Body Problem, AAS/AIAA Space Flight Mechanics Meeting, AAS 05-221, Copper Mtn., CO, 2005.
[41] R. L. Anderson, M. W. Lo, Virtual Exploration by Computing Global Families of Trajectories with Supercomputers, AAS/AIAA Space Flight Mechanics Conference, AAS 05-220, Copper Mtn., CO, 2005.
[42] H. Poincaré, Les Méthodes Nouvelles de la Mécanique Céleste, Gauthier-Villars, Paris, 1892.
[43] R. L. Anderson, J. S. Parker, Comparison of Low-Energy Lunar Transfer Trajectories to Invariant Manifolds, AAS/AIAA Astrodynamics Specialist Conference, AAS 11-423, Girdwood, AK, 2011.
[44] V. Szebehely, Theory of Orbits: The Restricted Problem of Three Bodies, Academic Press, New York, 1967, pp. 7-41.
[45] D. L. Richardson, N. D. Cary, A Uniformly Valid Solution for Motion About the Interior Libration Point of the Perturbed Elliptic-Restricted Problem, AAS 75-021, AAS/AIAA Astrodynamics Specialist Conference, Nassau, Bahamas, 1975.
[46] K. C. Howell, J. V. Breakwell, Three-Dimensional, Periodic, 'Halo' Orbits, Celestial Mechanics 32 (1) (1984) 53–71.
[47] S. Wiggins, Introduction to Applied Nonlinear Dynamical Systems and Chaos, 2nd Edition, Vol. 2 of Texts in Applied Mathematics, Springer-Verlag, New York, 2003, pp. 28-70.
[48] A. E. Roy, M. W. Ovenden, On the Occurrence of Commensurable Mean Motions in the Solar System. The Mirror Theorem, Monthly Notices of the Royal Astronomical Society 115 (1955) 296–309.
[49] A. Miele, Theorem of Image Trajectories in the Earth-Moon Space, Astronautica Acta 6 (51) (1960) 225–232.
[50] T. Parker, L. O. Chua, Practical Numerical Algorithms for Chaotic Systems, Springer-Verlag, New York, 1989, pp. 130-166.
[51] E. Fehlberg, Classical Fifth-, Sixth-, Seventh-, and Eighth-Order Runge-Kutta Formulas with Stepsize Control, Tech. Rep. NASA TR R-287 (Oct. 1968).
[52] L. F. Shampine, M. K. Gordon, Computer Solution of Ordinary Differential Equations, W. H. Freeman and Company, San Francisco, 1975.
[53] W. M. Folkner, J. G. Williams, D. H. Boggs, The Planetary and Lunar Ephemeris DE421, Tech. Rep. IOM 343R-08-003, Jet Propulsion Lab. (2008).
[54] C. D. Murray, S. F. Dermott, Solar System Dynamics, Cambridge University Press, Cambridge, United Kingdom, 1999, pp. 421-428.
[55] E. Barrabés, G. Gómez, Spatial p-q Resonant Orbits of the RTBP, Celestial Mechanics 84 (2002) 387–407.
[56] E. Barrabés, G. Gómez, Three-Dimensional p-q Resonant Orbits Close to Second Species Solution, Celestial Mechanics 85 (2003) 145–174.
[57] C. Conley, Low Energy Transit Orbits in the Restricted Three-Body Problem, SIAM Journal of Applied Mathematics 16 (1968) 732–746.
[58] R. L. Anderson, J. S. Parker, Survey of Ballistic Transfers to the Lunar Surface, Journal of Guidance, Control, and Dynamics 35 (4) (2012) 1256–1267.